

# Effect of Amino Acid Sequence and pH on Nanofiber Formation of Self-Assembling Peptides EAK16-II and EAK16-IV

Yooseong Hong,<sup>†</sup> Raymond L. Legge,<sup>†</sup> S. Zhang,<sup>‡</sup> and P. Chen<sup>\*,†</sup>

Department of Chemical Engineering, University of Waterloo, 200 University Avenue, Waterloo, Ontario, Canada N2L 3G1, and Center for Biomedical Engineering, Massachusetts Institute of Technology, Cambridge, Massachusetts 02139

Received May 7, 2003; Revised Manuscript Received June 24, 2003

Atomic force microscopy (AFM) and axisymmetric drop shape analysis-profile (ASDA-P) were used to investigate the mechanism of self-assembly of peptides. The peptides chosen consisted of 16 alternating hydrophobic and hydrophilic amino acids, where the hydrophilic residues possess alternating negative and positive charges. Two types of peptides, AEAEAKAKAEAEAKAK (EAK16-II) and AEAEAEAE-AKAKAKAK (EAK16-IV), were investigated in terms of nanostructure formation through self-assembly. The experimental results, which focused on the effects of the amino acid sequence and pH, show that the nanostructures formed by the peptides are dependent on the amino acid sequence and the pH of the solution. For pH conditions around neutrality, one of the peptides used in this study, EAK16-IV, forms globular assemblies and has lower surface tension at air–water interfaces than another peptide, EAK16-II, which forms fibrillar assemblies at the same pH. When the pH is lowered below 6.5 or raised above 7.5, there is a transition from globular to fibrillar structures for EAK16-IV, but EAK16-II does not show any structural transition. Surface tension measurements using ASDA-P showed different surface activities of peptides at air–water interfaces. EAK16-II does not show a significant difference in surface tension for the pH range between 4 and 9. However, EAK16-IV shows a noticeable decrease in surface tension at pH around neutrality, indicating that the formation of globular assemblies is related to the molecular hydrophobicity.

## Introduction

There is considerable interest in the relationship between protein conformation and function.<sup>1–5</sup> In particular, the state of aggregation or assembly of proteins may have a serious impact on their function. Numerous studies have revealed that a common mechanism of various types of protein-related physiological disorders, such as Alzheimer's, Parkinson's, Down's syndrome, Huntington's, prion diseases, and amyloidoses, appears to be related to abnormal protein folding and aggregation.<sup>6–10</sup> Alzheimer's disease, for example, is characterized by the presence of amyloid fibrils from the  $\beta$ -amyloid protein and the assemblies of fibrils and plaques in the brain. Prion diseases are thought to be due to conformational changes arising from the self-assembly of the prion proteins in the brain. A common feature of these conformational diseases is that they seem to result from the conversion of soluble and functional proteins into insoluble  $\beta$ -sheet-rich quaternary structures that are often fibrillar. This fact has motivated extensive research on the general mechanism of  $\beta$ -sheet formation and its aggregation or assembly to fibrillar quaternary structures. However, there is no study that has clearly demonstrated the mechanism of  $\beta$ -sheet formation and its aggregation or assembly.<sup>11–13</sup>

From a physicochemical perspective, there may be three major inter- and intramolecular forces that drive molecular self-assembly, namely, hydrogen bonding, hydrophobic, and electrostatic interactions. Hydrogen bonding is thought to be a determining factor in the formation of protein secondary structure. On the other hand, a number of processes in aqueous solution, such as protein folding or molecular recognition processes, strongly rely on the hydrophobic interactions. Electrostatic interactions can induce different protein conformations by changing the ionic state of the amino acid components.

To understand the mechanisms of protein/peptide self-assembly, we chose a model peptide that is simple but possesses all three physicochemical interactions. This peptide EAK16 is known to form unusually stable  $\beta$ -sheet structure.<sup>14–17</sup> This peptide has alternating hydrophobic (alanine (A)) and hydrophilic (glutamic acid (E) and lysine (K)) amino acids, where the hydrophilic residues form alternating negative and positive charges. This amino acid sequence was originally found in zuotin, a yeast protein, which binds left-handed Z-DNA preferentially.<sup>15</sup> It is known that peptides with alternating polar and nonpolar amino acid residues are able to adopt  $\beta$ -sheet structures;<sup>18</sup> this suggests that EAK16 may be useful as a model system for the study of fibril formation of  $\beta$ -amyloid.

Many factors can influence the behavior of peptide self-assembly, including (i) the amino acid sequence, (ii) concentration of the peptide, (iii) molecular size of the

\* To whom correspondence should be addressed. Phone: (519) 888-4567 x5586. Fax: (519) 746-4979. E-mail: p4chen@cape.uwaterloo.ca.

<sup>†</sup> University of Waterloo.

<sup>‡</sup> Massachusetts Institute of Technology.

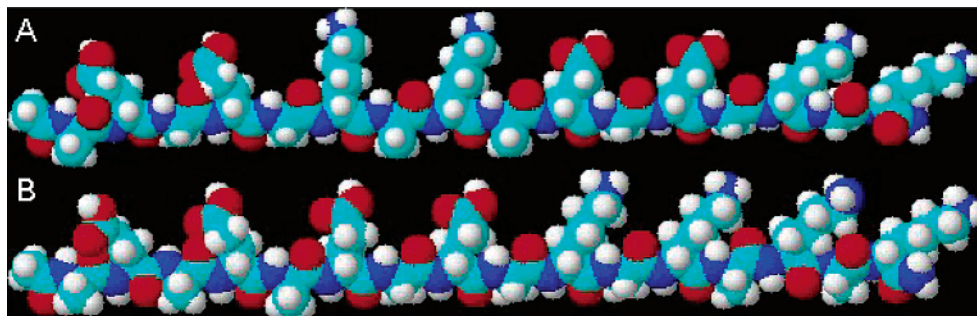


**Figure 1.** Schematic three-dimensional molecular model of EAK16-II, AEAEAKAKAEAEAKAK (A), and EAK16-IV, AEAEAEAEAKAKAKAK (B). Carbon atoms are cyan, oxygen atoms are red, nitrogen atoms are blue, and hydrogen atoms are white. In this conformation, all of the hydrophobic alanine side chains face in one direction, and all of the lysine and glutamic acid side chains face in the other direction to create two distinct faces. On the polar face, glutamic acid alternates with lysine.

peptide, (iv) pH of the solution, (v) temperature, (vi) the medium composition, such as solvent or substrate, (vii) ionic strength, and (viii) presence of denaturation agents, such as sodium dodecyl sulfate (SDS) and urea. This paper focuses on two factors: amino acid sequence and pH. The former is an intrinsic property of the peptide itself, and the latter is an environmental factor. By adjusting these two factors, the assemblies and conformational changes of EAK16 were investigated. Two types of EAK16 were used: EAK16-II that has an amino acid sequence of AEAEAKAKAEAEAKAK (N terminal to C terminal) and EAK16-IV that has a sequence of AEAEAEAEAKAKAKAK. The difference in the amino acid sequence makes these two EAK16s different in their charge distribution and hence polarity,  $- - + + - - + +$  for EAK16-II and  $- - - - + + + +$  for EAK16-IV.

The nanostructures of peptide assemblies were observed using atomic force microscopy (AFM). The AFM tapping mode was used in order to reduce sample surface distortion as a result of AFM tip and sample interactions.<sup>7</sup> Along with AFM, axisymmetric drop shape analysis-profile (ADSA-P) was employed to measure surface tension at the interface between water and air. By doing so, one can quantify the hydrophobicity, which is related to the conformation of the peptide assemblies. Surface tension can also be used to assess the surface activity of peptides<sup>19</sup> and kinetics of peptide adsorption.

### Materials and Methods

**Materials.** EAK16-II and EAK16-IV ( $C_{70}H_{121}N_{21}O_{25}$ , molecular weight 1657) were purchased from Research Genetics (Huntsville, AL), stored at 4 °C, and used without further purification. The N-terminus and C-terminus of these peptides were protected by acetyl and amino groups, respectively. Stock solutions of the peptides were prepared at concentrations of 0.2 mg/mL in water (18 MΩ; Millipore Milli-Q system) and stored at 4 °C before use. The stock solutions were diluted with pure water or buffer solution to a final peptide concentration of 0.1 mg/mL for AFM imaging. For pH studies, 40 mM phosphate buffers (sodium dihydrogen phosphate/sodium hydrogen phosphate pair,  $NaH_2PO_4/Na_2HPO_4$ ) in the pH range of 6.25–8.50 were used and mixed with the peptide stock solution to give a final peptide concentration of 0.1 mg/mL. Disodium phthalate buffer and

sodium carbonate buffer were used for the pH 4.0 and 11.0 solutions with a concentration of 40 mM, respectively. The EAK16s were incubated in buffer for 4 h prior to AFM imaging. For surface tension studies, the same sample preparation methods were applied. To test possible effects of impurities present in the peptide sample, peptides with high purity (>95%) were tested and the results were accompanied with those of the normal samples (see Results).

**Atomic Force Microscopy (AFM).** Approximately 10  $\mu$ L of the peptide solution was placed on the surface of a freshly cleaved mica sheet that was glued to a steel AFM sample plate. The sample was incubated for 1 h under the ambient conditions, then washed with approximately 50  $\mu$ L of pure water to remove unattached peptides and buffer components. After air-drying for 3 h, AFM imaging was performed at room temperature using the tapping mode on a PicoScan AFM (Molecular Imaging, Phoenix, AZ). All images were acquired by using a 225  $\mu$ m silicon single-crystal cantilever (type NCL, Molecular Imaging, Phoenix, AZ) with a typical tip radius of 10 nm and frequency of 165 kHz. A scanner with a maximum scan size of 6  $\mu$ m was used. Data sets were subjected to a first-order flattening.<sup>7,20</sup>

**Axisymmetric Drop Shape Analysis-Profile (ADSA-P).** A pendant drop of the peptide solution was formed at the tip of a vertical Teflon needle, connected to a motor-driven microsyringe. The sample was placed in a temperature-controlled environmental chamber, saturated with water vapor. The entire system was placed on a vibration-free table. The image of the pendant drop was acquired using an optical microscope and a CCD camera and then transferred to a computer. Software was used to digitize the image and generated a profile of the pendant drop. A theoretical curve, governed by the Laplace equation of capillarity, was then fitted to the profile, generating the surface tension value as a fitting parameter.<sup>21</sup>

### Results

**Self-Assembly of EAK16 in Pure Water.** Figure 1 shows the three-dimensional structures of EAK16-II and EAK16-IV using ChemSketch based on energy minimization.<sup>22</sup> Hydrophilic amino acid residues (lysine and glutamic acid) are located on one side, and hydrophobic amino acid residues (alanine) are located on the opposite side, generating two distinct hydrophilic and hydrophobic faces. Although the two

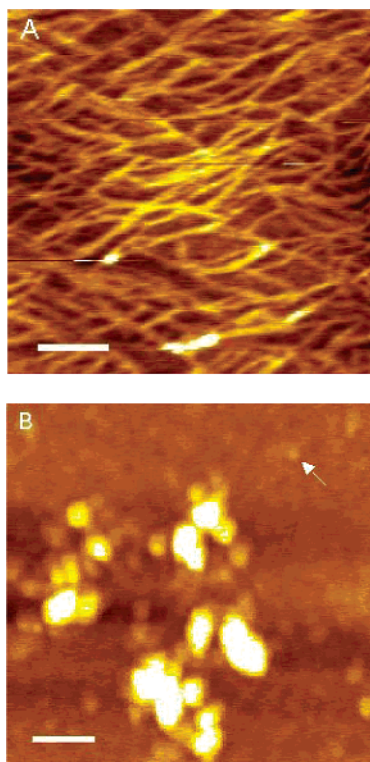


**Figure 2.** AFM images of EAK16-II (A) and EAK16-IV (B). EAK16-II forms fibrillar assemblies, whereas EAK16-IV forms globular assemblies. The width and height of each fibrillar assembly in part A is around 23 and 0.5 nm, respectively. The diameter and height of each globular assembly in part B is approximately 56 and 3 nm. Careful analysis of part B reveals that there are smaller globular assemblies (white arrow) in the background with a diameter and height of 34 and 1 nm, respectively. The scale bars are 200 nm. All lengths are corrected by considering the tip convolution effect.

peptides have the same amino acid composition, their amino acid sequences are different. EAK16-II has a charge sequence of  $- - + + - - + +$  at neutral pH, whereas, EAK16-IV has a charge sequence of  $- - - - + + + +$ . AFM images of these samples in aqueous solution are shown in Figure 2. A significant difference in nanostructure is seen between the two. EAK16-II forms fibrillar assemblies (Figure 2A), whereas EAK16-IV forms globular assemblies (Figure 2B). The fibrils of EAK16-II were observed repeatedly, regardless of the concentration of the peptide.<sup>23</sup> In addition, the fibrils of EAK16-II were also observed from the peptide with high purity (>95%). Because high purity peptide did not show significant differences compared to samples without purification, peptides were used as received without further purification.

In the analysis of dimensions of the assemblies, the widths may be broadened because of the convolution effects arising from the finite size of the AFM tip.<sup>7,20,24,25</sup> Thus, the observed dimensions have to be corrected. For a spherical sample with a radius of  $R_m$ , the observed width of the sample has a relationship,  $W_{\text{obs}} = 4(R_t R_m)^{1/2}$ , where  $R_t$  is the radius of the AFM tip.<sup>26–28</sup> When the sample is assumed to be a sheet, the real width of the sheet can be obtained by the following equation,  $W = W_{\text{obs}} - 2(2R_t H - H^2)^{1/2}$ , where  $H$  is the observed height.<sup>23</sup>

Figure 3 shows typical topographic images and their error signal (amplitude) images for both EAK16s with cross-

sectional profiles. The error signal is the difference between the force setpoint and the actual deflection of the cantilever.<sup>20</sup> This error signal matches with the topographic images. The EAK16-II fibril shown in the profile from the topographic image has a height of 0.5 nm and a width of 30 ~ 40 nm (Figure 3A). If the fibril is assumed to have a circular cross section, the observed width,  $W_{\text{obs}}$ , can be calculated with,  $4(R_t R_m)^{1/2}$ . Using the typical radius of the AFM tip of 10 nm and the height of the sample of 0.5 nm, the calculated value is 8.9 nm for the observed width. However, this value is much smaller than the actually observed value (30 nm). Therefore, the fibrils in the AFM image are not circular in cross section. When assuming that the fibrils are flat, like a sheet, an estimated width of 23 nm was obtained from the correction equation mentioned above. The corrected dimensions are used for all dimensions mentioned hereafter. Although the assemblies of EAK16-II are more like sheets, the term fibrils will still be used for consistency in terminology.

In the case of EAK16-IV assemblies, shown in the profile (Figure 3, parts C and D), the height and diameter are 2 and 60 nm, respectively. Using the same analysis as done for EAK16-II, the corrected diameter of the globular assembly was 48 nm, almost twice the width of the EAK16-II sheet. EAK16-IV forms very flat globular assemblies, like disks. There are also many smaller assemblies (white arrow in Figure 2B) in the background. These smaller assemblies have a height and diameter of 1 and 34 nm (corrected value), respectively. The height information does not require correction from the tip convolution effect. The height of the EAK16-IV assemblies is close to 2-fold of that of the EAK16-II assemblies. The accuracy in the height information of AFM images was verified using lipid bilayers.<sup>23</sup>

**Self-Assembly of EAK16s at Various pH Values.** The  $pK_a$  values of the side chains of glutamic acid and lysine are 4.25 and 10.53, respectively. Because the pH of the pure water is around 7, the carboxylic acid groups would be negatively charged and the amino groups positively charged. To test the effect of different ionic states of the amino acids on the formation of self-assembled nanostructures, a wide pH range was used, from pH 4 to pH 11. Two extreme pH conditions were tested first: pH 4 below the  $pK_a$  of glutamic acid, and pH 11 above the  $pK_a$  of lysine, so that either glutamic acid or lysine was neutralized. At these two pH values, both types of EAK16s showed the fibrillar assemblies (Figures 4 and 5A–N).

The nanostructures resulting from the self-assembling process were also observed at intermediate pHs (Figures 4 and 5B–M). Regardless of the values of pH, EAK16-II forms fibrils. However, EAK16-IV shows changes in nanostructure as a function of pH. EAK16-IV forms globular assemblies at pH between 6.5 and 7.5 but changes to fibrils at pHs below 6.5 or above 7.5.

To analyze the AFM images of EAK16-IV where globular assemblies were observed, the nanostructure was approximated as an ellipse with a major and minor axis. For a short segment of fibrils such as ones shown Figure 5, parts D, K, and L, the length of a short fibril was regarded as the length of its major axis and the width was regarded as the length



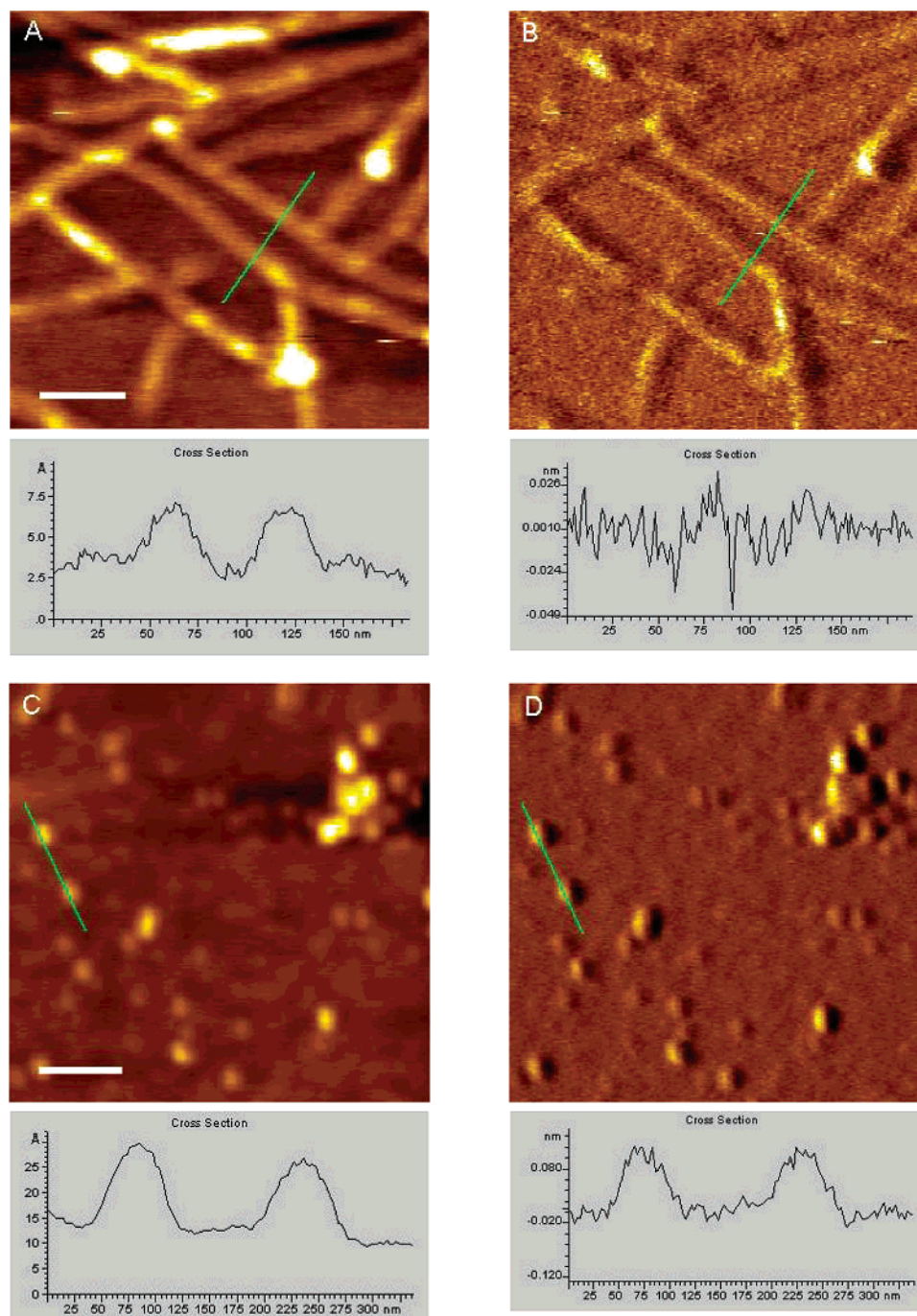


**Figure 3.** Typical AFM images of EAK16 and cross-section profiles for selected lines. (A) Topographic image (B) and error signal image for the corresponding area shown in part A for EAK16-II. C and D are for EAK16-IV. The error signal is the difference between the force setpoint and the actual deflection of the cantilever.<sup>21</sup> The heights are shown in the horizontal profile, which are 0.5 and 2 nm, respectively. The scale bars are (A) 100 nm and (C) 200 nm.

of its minor axis. The ratio of the length of the major axis to that of the minor axis was calculated from AFM images shown in Figure 5 and plotted, to determine if a structural transition was present. If this ratio was calculated for the long fibrils EAK16-II, it would be infinity at every pH value. The plot of the ratio for the assemblies of EAK16-IV is given in Figure 6. It is apparent that the nanostructure resulting from the self-assembly of EAK16-IV undergoes a transition from globular assemblies at moderate pH values to fibrillar networks at pHs below 6.5 or above 7.5. Errors were obtained from the ratio calculations on different assemblies for a given pH. Standard deviations of 10% were typical from the

measurements. The large error limits at pH 6.55, 7.60, and 7.90 suggest that at these pH values, short fibrillar segments coexist with long fibrils.

The dimensions of both EAK16 assemblies at various pH values are summarized in Table 1. For the EAK16-II assemblies, the average height and width of the fibrils is  $0.66 \pm 0.12$  and  $29.65 \pm 2.37$  nm, respectively. For the globular EAK16-IV assemblies, the average height, and the ratio of the major length to the minor length are  $2.22 \pm 0.25$  and  $1.26 \pm 0.17$  nm, respectively. The fibrillar assemblies of EAK16-IV at pHs below 6.5 or above 7.5 have a height and width of  $0.54 \pm 0.06$  and  $28.69 \pm 2.27$  nm, respectively,

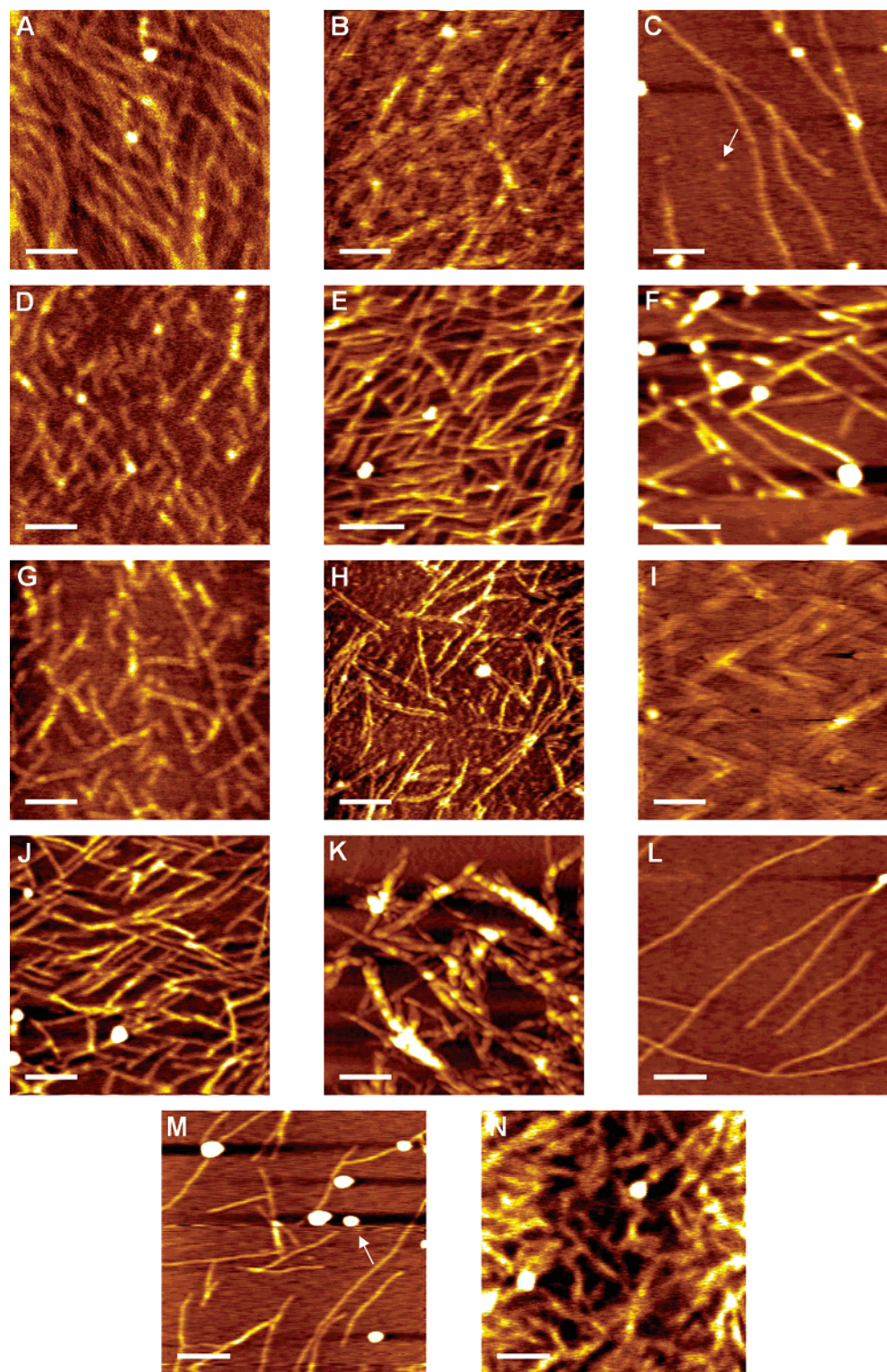


**Figure 4.** AFM images of EAK16-II at various pH values. (A) pH 4, (B) pH 6.25, (C) pH 6.40, (D) pH 6.55, (E) pH 6.70, (F) pH 6.85, (G) pH 7.00, (H) pH 7.15, (I) pH 7.30, (J) pH 7.45, (K) pH 7.60, (L) pH 7.90, (M) pH 8.50, and (N) pH 11. AFM images of EAK16-II at various pH values. All of the scale bars represent 200 nm.

which are very similar to those of EAK16-II assemblies. The assemblies of EAK16-IV at pH 4 (Figure 5A) were not taken into account, because they showed different features from the rest. These assemblies are like twisted ribbons so that their heights are significantly larger than the others. The twisted structures of ribbons may be related to the chirality of the amino acids.<sup>29–31</sup>

The fibrillar assemblies show several variations, including

the fibrils of EAK16-IV at pH 4, which are like twisted ribbons. Some of the fibrillar assemblies appear to be from the linear assemblies of the globules (Figure 4, parts G and K). There are also double or triple strands of fibrils, which pair to form bundles (Figure 4, parts B and I), resembling DNA bundling and collagen triple helix formation. Although the fibrillar assemblies are predominant, the small globules can be found in the background of the fibril networks or



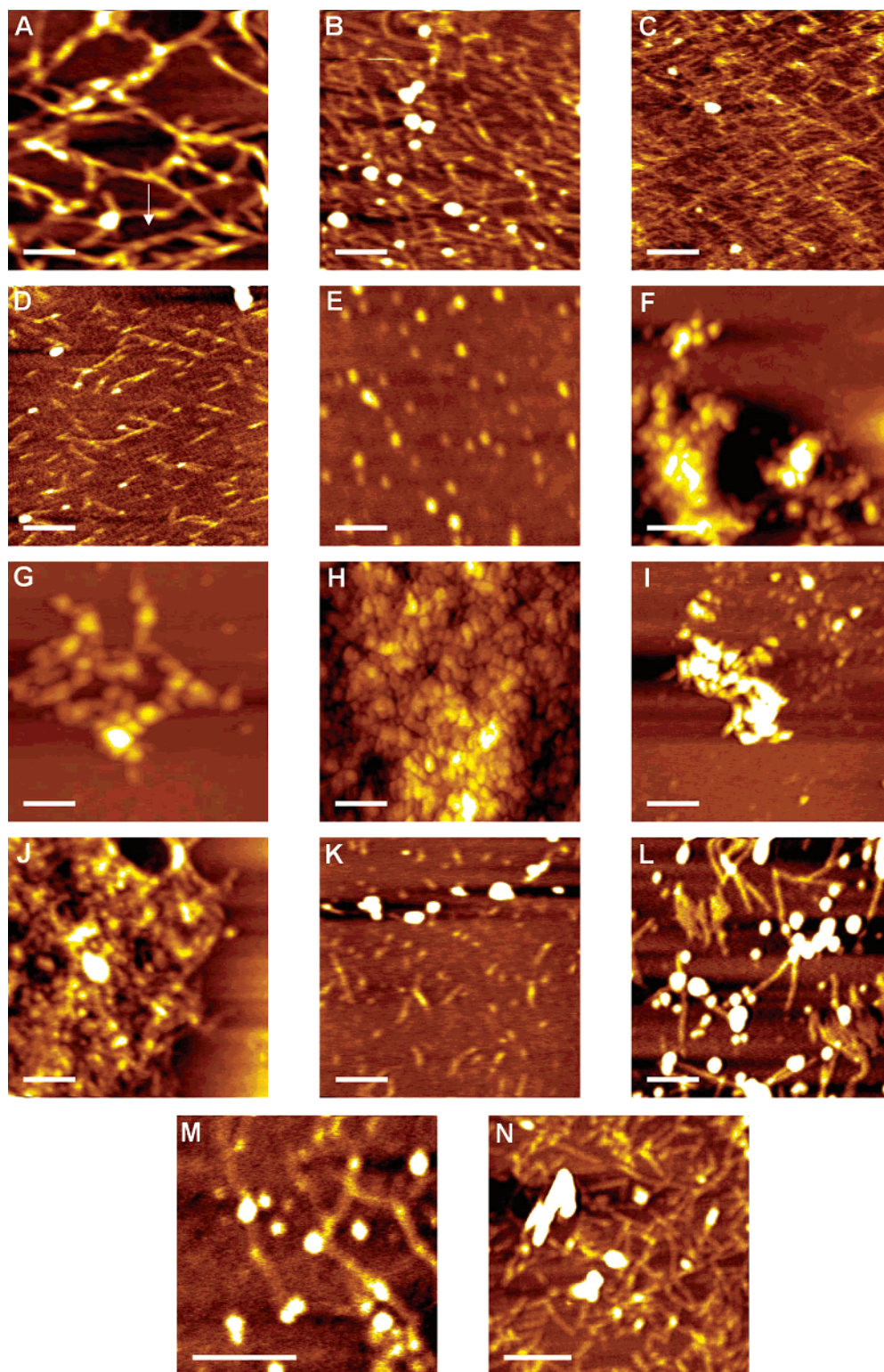


**Figure 5.** AFM images of EAK16-IV at various pH values. (A) pH 4, (B) pH 6.25, (C) pH 6.40, (D) pH 6.55, (E) pH 6.70, (F) pH 6.85, (G) pH 7.00, (H) pH 7.15, (I) pH 7.30, (J) pH 7.45, (K) pH 7.60, (L) pH 7.90, (M) pH 8.50, and (N) pH 11. AFM images of EAK16-IV at various pH values. The white arrow in part A shows the conformational feature of the twisted ribbon (note the different contrast in color). All of the scale bars represent 200 nm.

inside the fibrillar assemblies (Figure 4, parts C, G, H, K, and M). These small globular assemblies may function as a seed or nucleus for fibril formation, which was observed for Alzheimer's  $\beta$ -amyloid peptide.<sup>32</sup>

For EAK16-IV at low or high pHs, many large globules (bright spots in Figure 5, parts B, L, and M) are found. They are different from the globular assemblies of the peptide at

near neutral pHs. These relatively high globules (height > 10 nm) resemble the aggregates of buffer components, when the AFM images of buffer solution without peptides (data not shown) are compared.

#### Surface Tension of EAK16-II and EAK16-IV Solution.

Surface tension of the peptides can give information on their hydrophobicity in solution. It is expected that increased

Table 1. Dimensions of EAK16 Assemblies<sup>a</sup>

PH	EAK16-II			EAK16-IV		
	shape <sup>b</sup>	height	width	shape <sup>b</sup>	height	ratio <sup>c</sup>
4.00	F	0.68 ± 0.08	35.22 ± 4.22	F	3.20 ± 0.49	infinite
6.25	F	0.47 ± 0.06	19.67 ± 7.74	F	0.48 ± 0.08	infinite
6.40	F	0.40 ± 0.05	24.63 ± 3.19	F	0.41 ± 0.04	infinite
6.55	F	0.36 ± 0.06	37.51 ± 1.75	M	0.57 ± 0.05	4.73 ± 1.81
6.70	F	0.59 ± 0.08	24.36 ± 6.05	G	2.02 ± 0.25	1.28 ± 0.15
6.85	F	0.63 ± 0.06	32.09 ± 2.02	G	2.48 ± 0.86	1.20 ± 0.16
7.00	F	0.55 ± 0.07	29.07 ± 3.43	G	2.35 ± 0.69	1.17 ± 0.12
7.15	F	0.72 ± 0.06	28.06 ± 6.59	G	2.05 ± 0.31	1.32 ± 0.21
7.30	F	0.42 ± 0.06	26.33 ± 4.15	G	2.12 ± 0.45	1.28 ± 0.19
7.45	F	0.64 ± 0.09	30.40 ± 3.06	G	2.32 ± 0.45	1.32 ± 0.16
7.60	F	1.90 ± 0.29	30.88 ± 3.93	M	0.43 ± 0.09	2.69 ± 1.12
7.90	F	0.47 ± 0.09	23.52 ± 2.68	M	1.18 ± 0.19	6.70 ± 2.88
8.50	F	0.53 ± 0.09	27.16 ± 4.59	F	0.64 ± 0.08	infinite
11.00	F	0.78 ± 0.12	37.78 ± 3.37	F	0.66 ± 0.12	infinite
average	F	0.66 ± 0.12	29.65 ± 2.37	F <sup>d</sup>	0.54 ± 0.06	infinite
				G	2.22 ± 0.25	1.26 ± 0.17

<sup>a</sup> 95% confidence intervals are shown. Heights are obtained by AFM software, and the widths and other lengths are measured and corrected. All units are in nanometers (top panel). Average dimensions of EAK16-II and -IV assemblies in buffer solution; 95% confidence intervals are shown. The ribbonlike assemblies of EAK16-IV at pH 4 are not taken into account because of these unique nanostructures (bottom panel). <sup>b</sup> F, fibrillar assemblies; G, globular assemblies; and M, short fibrillar aggregates, which are not long enough to be regarded as fibrillar assemblies. <sup>c</sup> Ratio = the ratio of the major to minor length of globular assemblies. <sup>d</sup> The fibrillar assemblies of EAK16-IV have an average width of 28.69 ± 2.27 nm.

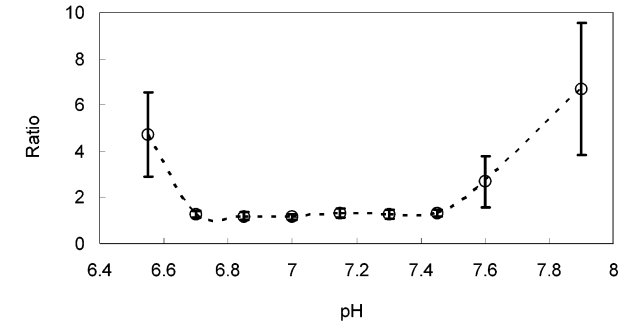


Figure 6. Plot of the ratio of the major to minor length of nanostructures of EAK16-IV with respect to pH from the data in Table 1. Error bar shows 95% confidence interval.

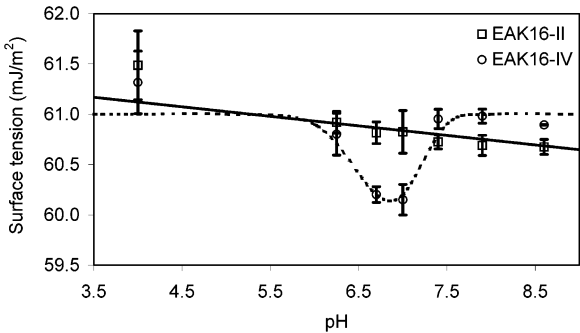


Figure 8. Surface tension of EAK16-II and EAK16-IV as a function of pH. The average method was used to estimate surface tension from dynamic surface tension measurement. Straight and dotted lines are used to guide the eye for the trend for EAK16-II and -IV, respectively.

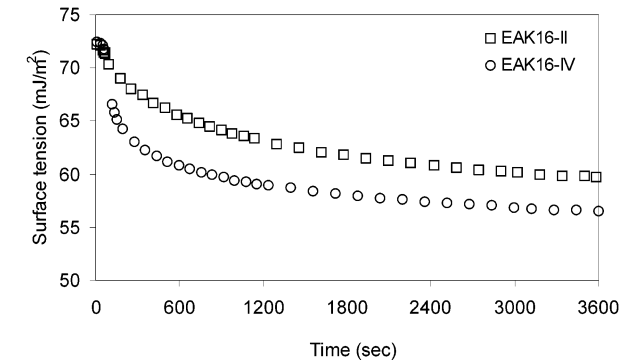


Figure 7. Surface tension of EAK16-II and EAK16-IV aqueous solutions as a function of time. Dynamic surface tension values are measured for 1 h. Standard deviation of each experiment is less than 0.2 mJ/m<sup>2</sup>.

hydrophobicity would lead to increased surface activity at the air–water interface, resulting in decreased surface tension.<sup>33</sup> This information on hydrophobicity makes it possible to speculate on the conformation of the assemblies of peptide. Figure 7 shows surface tension measurements as a function of time for EAK16-II and EAK16-IV aqueous solutions; EAK16-IV has a lower surface tension than EAK16-II. Because EAK16-II and EAK16-IV do not reach

a plateau that corresponds to the equilibrium state within a reasonable experimental duration, an approximation method was necessary to estimate equilibrium surface tension. Among several known methods to estimate the equilibrium surface tension,<sup>34–36</sup> the average method was used. In the average method, the final 15 data points were averaged to give a representative surface tension value. Because the surface tension of each EAK16 solution was measured for 1 h, this averaged value for the final 15 data points is thought to be comparable to each other. Using this method, the equilibrium surface tension of EAK16-II is 59.766 ± 0.035 mJ/m<sup>2</sup>, whereas that of EAK16-IV is 56.578 ± 0.028 mJ/m<sup>2</sup>.

Figure 8 shows the estimated equilibrium surface tensions of EAK16-II and EAK16-IV at different pH values. EAK16-II does not show a significant change in surface tension over the range of pHs, whereas EAK16-IV shows significantly lower surface tensions at pHs around 6.7. The nanostructures of EAK16-II do not show any significant change with respect to pH, which may be related to the almost constant surface tension that is observed. In contrast, EAK16-IV shows globular assemblies at pHs between 6.5 and 7.5, and fibrillar assemblies at pHs below 6.5 or above 7.5. Correspondingly,

the surface tensions of EAK16-IV are lower at pHs between 6.7 and 7.0 than those at pHs below 6.5 or above 7.5.

Because the surface tension was tested in buffer, it is necessary to consider the effect of buffer components on surface tension of the solution. Surface tensions of the pure buffer solutions showed the same value as pure water (data not shown). Therefore, the buffer does not affect the surface tension measurements; the differences in surface tension are attributed to the innate properties of these peptides.

## Discussion

AFM observations and surface tension measurements suggest that changes in pH of the environment cause significant differences in the resulting peptide nanostructures. Moreover, different amino acid sequences give different nanostructures as well as different surface activity. Both of the EAK16s studied in this work have the capability of hydrogen bonding and hydrophobic interactions, as well as electrostatic interactions. The  $\beta$ -sheets of self-assembling peptides are believed to form through hydrogen bonding and to be stabilized by hydrophobic and electrostatic interactions.<sup>14–17</sup> However, there are differences in nanostructure between EAK16-II and EAK16-IV, even though both are known to form  $\beta$ -sheets.<sup>14,16</sup> In this study, the different charge distribution or polarity of the peptides appears to play the most important role in forming different structures of assemblies. According to the experimental observations regarding nanostructures, it can be concluded that the reduction of electrostatic interactions does facilitate nanofiber formation with certain amino acid sequences, which is comparable with what has been observed in other studies.<sup>37,38</sup> In the case of EAK16-IV, for example, the reduction or removal of electrostatic interactions at pH 4 or pH 11 because of the neutralization of one of the ionizable side groups of amino acids, glutamic acid, and lysine, induced the conformational change from globular assemblies at near neutral pHs to fibrillar ones at low (e.g., pH 4) or high pHs (e.g., pH 11). In contrast, EAK16-II formed fibrillar assemblies within all pH ranges we used (pH 4 ~ pH 11). Although both peptides have considerable similarity in the degree of hydrogen bonding and hydrophobic interactions, the slight increase in electrostatic interactions because of the different charge distribution appears to prevent EAK16-IV from forming nanofibers at neutral pHs. These observations show that the nanostructure can be modified by rearranging the amino acid sequence to give different charge distributions.

In addition to the different conformations, the assemblies of EAK16-II and EAK16-IV show different adhesion patterns on a mica surface. The fibrillar assemblies form networks that are evenly distributed over the mica surface, whereas the globular assemblies show localized clusters of globules. The fibrillar assemblies that are formed in bulk appear to adhere on hydrophilic mica surfaces preferentially possibly through the favorable interaction between hydrophilic-hydrophilic surfaces. Because the surface tension measurements show that the fibrillar assemblies are more hydrophilic compared to the globular assemblies, there may be a favorable interaction between hydrophilic fibrillar assemblies

and the mica surface. This may explain why networks of fibrillar assemblies of EAK16-II are observed on mica surfaces. In contrast, the globular assemblies, being more hydrophobic, seem to have stronger interactions with each other compared to the interactions with the hydrophilic mica surface. Thus, the clustered globular assemblies of EAK16-IV that form in bulk are observed on the mica surface. This observation also implies the unfavorable interaction between globular assemblies and the hydrophilic mica substrate.

The surface tension results show that EAK16-IV in pure water has a lower surface tension than EAK16-II, indicating that EAK16-IV assemblies are likely more hydrophobic. The difference in assembled nanostructures can be found in the AFM images. Those images show that EAK16-II forms fibrillar assemblies, whereas EAK16-IV forms globular assemblies in aqueous solution of near neutral pH. The height of the fibrillar assemblies of EAK16-II is approximately 0.5 nm, measured from the AFM images. This value is similar to the molecular width of EAK16-II and also close to the intersheet distance between  $\beta$ -sheets of poly(lysine), which is known to be 0.76~0.85 nm.<sup>39</sup> Therefore, it may be postulated that EAK16-II assemblies observed in the AFM images correspond to a single layer of  $\beta$ -sheet, because EAK16s are known to form  $\beta$ -sheets.<sup>14,16</sup>

The height of the globular assemblies of EAK16-IV is at least 1 nm based on AFM images, which corresponds to the height of two layers of  $\beta$ -sheet, or a folded  $\beta$ -sheet. Based on these experimental observations, we can speculate on the possible differences in the self-assembly mechanisms of EAK16-II and -IV. At intermediate pHs, EAK16-IV appears to have stronger intramolecular electrostatic attractions between the carboxylic acid groups of glutamic acid and amino acid groups of lysine than EAK16-II. This can occur as a result of the charge distribution, which develops toward the two ends of the molecule. Consequently, the EAK16-IV molecule may be able to bend or fold by such intramolecular attractive electrostatic interactions. In addition, Fourier transform infrared (FT-IR) spectrum of EAK16-IV at neutral pH indicated potential presence of  $\beta$ -turn structures.<sup>40</sup> As a result, the hydrophilic amino acids, glutamic acid, and lysine, form a hydrophilic core of the assembly because of strong electrostatic attraction, and the hydrophobic alanine groups are exposed outside. The hydrophobic exterior of EAK16-IV assemblies tends to lower the surface tension more significantly than the less hydrophobic exterior of EAK16-II assemblies. Furthermore, this unfavorable exposure of hydrophobic groups in aqueous solution makes EAK16-IV molecules or assemblies grow into larger globular assemblies through hydrophobic interactions with each other. Because of their larger size, fewer globular assemblies form. The globular assemblies of EAK16-IV are, therefore, not detected as frequently as the fibrillar assemblies of EAK16-II on mica surfaces (compare part E to I in Figures 4 and 5).

At pH 4, the carboxylic acid group of the glutamic acid becomes neutralized and the electrostatic attraction between glutamic acid and lysine becomes significantly weaker than that at pH 7. Thus, EAK16-IV may not have sufficient electrostatic attraction to cause bending of the molecule. Consequently, the straight EAK16-IV molecules form fibril-



lar assemblies, rather than globular assemblies (Figure 5A). Similarly, at pH 11, the amino groups of lysine are neutralized, reducing the electrostatic attraction between glutamic acid and lysine. This reduced electrostatic attraction is insufficient to cause the molecular bending; as a result, fibrillar assemblies are formed (Figure 5N). The surface tension of EAK16-IV at pH 4 is higher than those at nearly neutral pHs and shows no significant difference from that of EAK16-II (Figure 8). This also implies that EAK16-IV forms fibrillar assemblies at pH 4 like EAK16-II. It is significant that the surface tension of EAK16-II remains almost constant over a wide range of pHs, which is consistent with the nanostructures observed by AFM, where fibrils always exist. It is also significant that the surface tensions of EAK16-IV at pHs below 6.5 and above 7.5 do not show any noticeable variations. Nanostructures of EAK16-IV at these pHs are fibrillar. However, EAK16-IV does show lower surface tensions when the pH is between 6.5 and 7.5, which correspond to the formation of globular nanostructures. The surface tension differences are in good agreement with the nanostructure differences.

Our speculations regarding the formation of fibrillar and globular assemblies seem to be contradictory to the mechanism proposed by Altman et al.<sup>14</sup> They proposed a mechanism of peptide self-assembly based on fiber formation of peptides. In their proposed mechanism, the peptides adopt an extended-strand conformation that undergoes self-assembly, which can be used to explain the fiber formation. With this mechanism, however, it is difficult to explain how the globular assemblies form, which we observed with EAK16-IV at neutral pHs. To explain the difference nanostructures formed by the two peptides, EAK16-II and -IV, it is necessary to consider the difference in the structural properties of two peptides, which has not accounted for in Altman et al. proposed mechanism. Of the differences between the two peptides, charge distribution seems to play a key role in determining their nanostructures. A recent Fourier transform infrared (FT-IR) experiment<sup>40</sup> has shown existence of a  $\beta$ -turn in the secondary structure of EAK16-IV at neutral pH, but not in the secondary structure of EAK16-II. This result would suggest the possibility of molecular bending of EAK16-IV,<sup>40</sup> in contrast to the conformation for EAK16-II, which showed predominately  $\beta$ -sheet structure.<sup>40</sup> Incorporating this additional information into the present observations on the globular assemblies, we believe that it is plausible to propose a mechanism involving the bending of EAK16-IV at neutral pHs. Future work should include detailed studies, such as X-ray crystallography and nucleic magnetic resonance (NMR), on the molecular properties of these peptides to confirm these speculations or develop a more convincing mechanism to explain the differences in peptide self-assembly.

It is worth noting that the conformational change of EAK16-IV is related to its pI (calculated at  $\sim 6.71$ ).<sup>16</sup> EAK16-IV forms globular assemblies and shows lower surface tension near its pI, whereas it forms fibrillar assemblies and shows relatively high surface tension below pH 6.5 or above pH 7.5. An implication of this observation is that it is possible to control the resulting nanostructure

and hydrophobicity of peptide assemblies by selecting amino acid components to have the desired pI. For example, the use of arginine ( $pK_a = 12.48$ ) instead of lysine ( $pK_a = 10.53$ ) would be expected to make the peptide undergo the conformational transition at a higher pH than EAK16-IV (pH  $\sim 7.5$ ). The observations here suggest that the nanostructure and organization of these peptides can be controlled and modified by the adjustment of the amino acid sequence or the pH of the solution.

## Summary

In this study, the effects of the amino acid sequence and pH on the nanostructures resulting from the self-assembly of peptides were investigated. Under moderate pH conditions, pHs between 6.5 and 7.5, EAK16-IV forms globular assemblies, whereas EAK16-II forms fibrils. When the pH of the solution is below 6.5 or above 7.5, the nanostructures formed by EAK16-IV change from globules to fibrils. In contrast, the nanostructure of self-assembling EAK16-II does not show a drastic change within the entire pH range of 4.0 to 11.0. In addition, the globular assemblies of EAK16-IV show lower surface tension than the fibrillar assemblies. The different shapes and properties of the assemblies are due to differences in charge distribution between EAK16-II and EAK16-IV. These results illustrate that the nanostructures resulting from the self-assembly of EAK16 can be controlled and modified readily by adjustment of amino acid sequence and pH. The differences in amino acid sequence also are reflected in the surface activity of the peptides. The formation of different nanostructures can be further explored to modify and design various forms of nanostructures using self-assembly of peptides.

**Acknowledgment.** We thank Dr. Jean Duhamel, Shane Fung, Christine Keyes, and Jeremy Bezaire for helpful discussions. This research was financially supported by the Natural Sciences and Engineering Research Council of Canada (NSERC), Canadian Foundation for Innovation (CFI), and the Premier's Research Excellence Award (PREA).

## References and Notes

- (1) Good, T. A.; Murphy, R. M. Aggregation state-dependent binding of  $\beta$ -amyloid peptide to protein and lipid components of rat cortical homogenates. *Biochem. Biophys. Res. Commun.* **1995**, *207*, 209–215.
- (2) Kelly, J. W. Alternative conformations of amyloidogenic proteins govern their behavior. *Curr. Opin. Struct. Biol.* **1996**, *6*, 11–17.
- (3) Kelly, J. W. The environmental dependency of protein folding best explains prion and amyloid diseases. *Proc. Natl. Acad. Sci. U.S.A.* **1998**, *95*, 930–932.
- (4) Simmons, L. K.; May, P. C.; Tomaselli, K. J.; Rydel, R. E.; Fuson, K. S.; Brigham, E. F.; Wright, S.; Lieberburg, I.; Becker, G. W.; Brems, D. N. Secondary structure of amyloid  $\beta$  peptide correlates with neurotoxic activity in vitro. *Mol. Pharmacol.* **1994**, *45*, 373–379.
- (5) Wu, S. K.; Zeng, K.; Wilson, I. A.; Balch, W. E. Structural insights into the function of the Rab GDI superfamily. *Trends Biochem. Sci.* **1996**, *21*, 472–476.
- (6) Carrell, R. W.; Lomas, D. A. Conformational disease. *Lancet* **1997**, *350*, 134–138.
- (7) Chamberlain, A. K.; MacPhee, C. E.; Zurdo, J.; Morozova-Roche, L. A.; Hill, H. A.; Dobson, C. M.; Davis, J. J. Ultrastructural organization of amyloid fibrils by atomic force microscopy. *Biophys. J.* **2000**, *79*, 3282–3293.

- (8) Kelly, J. W.; Lansbury, P. T., Jr. A chemical approach to elucidate the mechanism of transthyretin and  $\beta$ -protein amyloid fibril formation. *Amyloid* **1994**, *1*, 186–205.
- (9) Pan, K. M.; Baldwin, M.; Nguyen, J.; Gasset, M.; Serban, A.; Groth, D.; Mehlhorn, I.; Huang, Z.; Fletterick, R. J.; Cohen, F. E. Conversion of  $\alpha$ -helices into  $\beta$ -sheets features in the formation of the scrapie prion proteins. *Proc. Natl. Acad. Sci. U.S.A.* **1993**, *90*, 10962–10966.
- (10) Fraser, P. E.; McLachlan, D. R.; Surewicz, W. K.; Mizzen, C. A.; Snow, A. D.; Nguyen, J. T.; Kirschner, D. A. Conformation and fibrillogenesis of Alzheimer  $A\beta$  peptides with selected substitution of charged residues. *J. Mol. Biol.* **1994**, *244*, 64–73.
- (11) Hwang, W.; Marini, D. M.; Kamm, R. D.; Zhang, S. Supramolecular structure of helical ribbons self-assembled from a  $\beta$ -sheet peptide. *J. Chem. Phys.* **2003**, *118*, 389–397.
- (12) Balbirnie, M.; Grothe, R.; Eisenberg, D. S. An amyloid-forming peptide from the yeast prion Sup35 reveals a dehydrated  $\beta$ -sheet structure for amyloid. *Proc. Natl. Acad. Sci. U.S.A.* **2001**, *98*, 2375–2380.
- (13) Kaye, R.; Bernhagen, B.; Greenfield, N.; Sweimeh, K.; Brunner, H.; Voelter, W.; Kapurniotu, A. Conformational transitions of islet amyloid polypeptide (IAPP) in amyloid formation in vitro. *J. Mol. Biol.* **1999**, *287*, 781–796.
- (14) Altman, M.; Lee, P.; Rich, A.; Zhang, S. Conformational behavior of ionic self-complementary peptides. *Protein Sci.* **2000**, *9*, 1095–1105.
- (15) Zhang, S.; Holmes, T.; Lockshin, C.; Rich, A. Spontaneous assembly of a self-complementary oligopeptide to form a stable macroscopic membrane. *Proc. Natl. Acad. Sci. U.S.A.* **1993**, *90*, 3334–3338.
- (16) Zhang, S.; Lockshin, C.; Cook, R.; Rich, A. Unusually stable  $\beta$ -sheet formation in an ionic self-complementary oligopeptide. *Biopolymers* **1994**, *34*, 663–672.
- (17) Zhang, S.; Altman, M. Peptide self-assembly in functional polymer science and engineering. *React. Funct. Polym.* **1999**, *41*, 91–102.
- (18) Brack, A.; Orgel, L. E.  $\beta$  structures of alternating polypeptides and their possible prebiotic significance. *Nature* **1975**, *256*, 383–387.
- (19) Chen, P.; Lahooti, S.; Policova, Z.; Cabrerizo-Vilchez, M. A.; Neumann, A. W. Concentration dependence of the film pressure of human serum albumin at the water/decane interface. *Colloids Surf. B: Biointerfaces* **1996**, *6*, 279–289.
- (20) Forbes, J. G.; Jin, A. J.; Wang, K. Atomic force microscope study of the effect of the immobilization substrate on the structure and force-extension curves of a multimeric protein. *Langmuir* **2001**, *17*, 3067–3075.
- (21) Lahooti, S.; del Rio, O. I.; Cheng, P.; Neumann, A. W. In *Applied Surface Thermodynamics*; Neumann, A. W., Spelt, J. K., Eds.; Marcel Dekker: New York, 1996; pp 441–507.
- (22) <http://www.acdlabs.com>.
- (23) Fung, S. Y.; Keyes, C.; Duhamel, J.; Chen, P. Concentration effects on the aggregation of a self-assembling oligopeptide. *Biophys. J.* **2003**, *85*, 537–548.
- (24) Goldsbury, C.; Kistler, J.; Aebi, U.; Arvinte, T.; Cooper, G. J. S. Watching amyloid fibrils grow by time-lapse atomic force microscopy. *J. Mol. Biol.* **1999**, *285*, 33–39.
- (25) Ionescu-Zanetti, C.; Khurana, R.; Gillespie, J. R.; Petrick, J. S.; Trabachino, L. C.; Minert, L. J.; Carter, S. A.; Fink, A. L. Monitoring the assembly of Ig light-chain amyloid fibrils by atomic force microscopy. *Proc. Natl. Acad. Sci. U.S.A.* **1999**, *96*, 13175–13179.
- (26) Gale, M.; Pollanen, M. S.; Markiewicz, P.; Goh, M. C. Sequential assembly of collagen revealed by atomic force microscopy. *Biophys. J.* **1995**, *68*, 2124–2128.
- (27) Markiewicz, P.; Goh, M. C. Atomic force microscopy probe tip visualization and improvement of images using a simple deconvolution procedure. *Langmuir* **1994**, *10*, 5–7.
- (28) Vesenka, J.; Guthold, M.; Tang, C. L.; Keller, D.; Delaine, E.; Bustamante, C. Substrate preparation for reliable imaging of DNA molecules with the scanning force microscope. *Ultramicroscopy* **1992**, *42–44*, 1243–1249.
- (29) Marini, D. M.; Hwang, W.; Lauffenburger, D. A.; Zhang, S.; Kamm, R. D. Left-handed helical ribbon intermediates in the self-assembly of a  $\beta$ -sheet peptide. *Nano Lett.* **2002**, *2*, 295–299.
- (30) Nyrkova, I. A.; Semenov, A. N.; Aggeli, A.; Boden, N. Fibril stability in solutions of twisted  $\beta$ -sheet peptides: a new kind of micellization in chiral systems. *Eur. Phys. J. B.* **2000**, *17*, 481–497.
- (31) Zhang, Y. J.; Jin, M.; Lu, R.; Song, Y.; Jiang, L.; Zhao, Y.; Li, T. J. Interfacial-dependent morphologies in the self-organization system of chiral molecules observed by atomic force microscopy. *J. Phys. Chem. B* **2002**, *106*, 1960–1967.
- (32) Seilheimer, B.; Bohrmann, B.; Bondolfi, L.; Muller, F.; Stuber, D.; Dobeli, H. The toxicity of the Alzheimer's  $\beta$ -amyloid peptide correlates with a distinct fiber morphology. *J. Struct. Biol.* **1997**, *119*, 59–71.
- (33) Magdassi, S.; Garti, N. In *Interfacial Phenomena in Biological Systems*; Bender, M., Ed.; Marcel Dekker: New York, 1991; pp 289–299.
- (34) Applequist, J.; Dorty, P. In *Polyamino acids, polypeptides and proteins*; Stahmann, M. A., Ed.; University of Wisconsin: Wisconsin, 1962; pp 161–171.
- (35) Miller, R.; Kretzschmar, G. Adsorption kinetics of surfactants at fluid interfaces. *Adv. Colloid Interface Sci.* **1991**, *37*, 97–121.
- (36) Miller, R.; Lunkenheimer, K. On the determination of equilibrium surface tension values of surfactant solutions. *Colloid Polym. Sci.* **1983**, *261*, 585–590.
- (37) Caplan, M. R.; Moore, P. N.; Zhang, S.; Kamm, R. D.; Lauffenburger, D. A. Self-assembly of a  $\beta$ -sheet protein governed by relief of electrostatic repulsion relative to van der Waals attraction. *Biomacromolecules* **2000**, *1*, 627–631.
- (38) Caplan, M. R.; Schwartzfarb, E. M.; Zhang, S.; Kamm, R. D.; Lauffenburger, D. A. Control of self-assembling oligopeptide matrix formation through systematic variation of amino acid sequence. *Biomaterials* **2002**, *23*, 219–227.
- (39) Fraser, R. D. B.; MacRae, T. P. *Conformation in Fibrous Proteins*; Academic Press: New York, 1973; pp 218–246.
- (40) Hong, Y.; Legge, R. L.; Chen, P. unpublished results.

BM0341374